Molecule-Dependent Plasmonic Enhancement of Fluorescence and Raman Scattering near Realistic Nanostructures

Andreas M. Kern,[†,‡,*] Alfred J. Meixner,[‡] and Olivier J. F. Martin[†,*]

[†]Nanophotonics and Metrology Laboratory, Swiss Federal Institute of Technology Lausanne (EPFL), 1015 Lausanne, Switzerland and [‡]Institute of Physical and Theoretical Chemistry, Eberhard Karls University, 72076 Tübingen, Germany

ABSTRACT

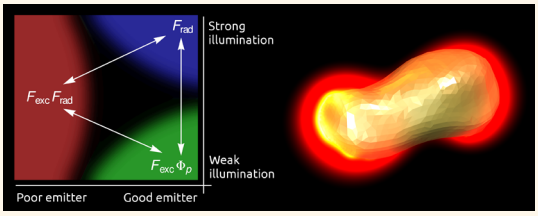

The enhancement of fluorescence and Raman scattering by plasmonic nanostructures is studied theoretically with special focus on the effects of the observed molecule's properties and the realistic geometry of the plasmonic nanostructure. Numerical experiments show that the enhancement factor may vary by many orders of magnitude depending on a fluorophore's transition rates or intrinsic quantum yield. For different molecules, boosting fluorescence enhancement means optimizing different factors, leading to a different ideal geometric and spectral configuration. This framework, coupled with powerful new simulation tools, will facilitate the design and characterization of fluorescence-enhancing plasmonic nanostructures as well as yield experimental access to the intrinsic properties of the molecules under study.

KEYWORDS: plasmonics · fluorescence enhancement · surface-enhanced Raman scattering · luminescence · realistic nanostructure · surface roughness · quantum yield

In the past decade, the localized enhancement of fluorescence processes and Raman scattering has materialized as a model application of plasmonic nanostructures.[1−16] Tuned to the right wavelength, such a nanostructure acts as an antenna, leading to an enhancement of the incident, exciting radiation as well as amplifying the light reemitted by the molecule. The obtained increase in signal can be used to make visible weak radiative processes, for example, in biological systems[17−20] or organic semiconductors.[21] To quantify the efficiency of this approach, an enhancement factor can be defined which compares the measurable signal, in most settings the optical power radiated to the far-field, for the case of a molecule near an enhancing structure with that of the same molecule in free space. The total enhancement factor is the result of a balance between various processes pertaining to both the excitation and reemission of light and depends on many properties of the molecule as well as the plasmonic structure.

Various models have been presented to predict the enhancement factors near rough metal surfaces[22] and metal nanoparticles.[23−26] These models give interesting insight into the factors which affect enhancement, but make assumptions regarding either the molecule's transition rates[25,26] or intrinsic quantum yield.[25] In addition, the effect of the plasmonic nanostructure is described using either empirical values[22,23] or a simplified analytical model.[17−19,25−27] While analytical models may produce elegant descriptions of complex phenomena and can aid in the comprehension of a process's physical background, numerical simulations are often unavoidable when considering a real-world scenario. In this study, we present a formalism which distills the properties of both the molecule and the plasmonic nanostructure into two unitless factors. This approach can be used to describe a wide range of molecules and plasmonic environments. With the factors chosen appropriately, we can reproduce the results of the previous models but also find settings in which considerably different results are to be expected. The presented formalism allows an optimal configuration for the position as well as the spectral tuning of the molecule with respect to the plasmonic particle to be determined. Paired with a numerical tool allowing the simulation of complex geometries,

* Address correspondence to a.kern@uni-tuebingen.de, olivier.martin@epfl.ch.

Received for review July 26, 2012 and accepted September 30, 2012.

Published online September 30, 2012
10.1021/nn3033612

the formalism can be applied to realistic systems. This information is important for the design and optimization of plasmonic nanostructures in single molecule fluorescence and Raman scattering applications, but can also aid in the interpretation of experimental results.

THEORETICAL BACKGROUND

Consider a quantum system such as a fluorescent molecule in free space, illuminated by a plane wave of wavelength λ_{exc} and intensity I^0. The Jablonski diagram of this system is shown in Figure 1. A molecule in the ground state $|g\rangle$ is excited to an intermediate excited state $|i\rangle$ by absorption of an incident photon. This process occurs with the transition rate γ_{abs}. From $|i\rangle$, the molecule quickly and nonradiatively decays to the excited state $|e\rangle$. Once in $|e\rangle$, the molecule can decay either radiatively or nonradiatively to the ground state $|g\rangle$. Intrinsic losses form a nonradiative decay channel with a decay rate of γ_{int}, while emission of a photon occurs with the decay rate γ_{em}. The emitted photon's wavelength λ_{em} is red-shifted with respect to λ_{exc} due to the energy lost in the $|i\rangle-|e\rangle$ transition.

Exciting the quantum system in proximity to a plasmonic nanostructure has two dominant effects on the transition rates described above. First, the enhancement of the incident light in the near-field of the nanostructure increases absorption by the molecule. The absorption rate can be written as $\gamma_{abs} = I\tilde{\sigma} = I\sigma/E_{abs}$ where I is the plasmonically enhanced incident intensity, σ is the absorption cross section of the $|g\rangle-|i\rangle$-transition and E_{abs} is the energy of the absorbed photons. Thus, the plasmonic particle causes an enhancement of the molecule's excitation by the factor

$$F_{exc} = I/I^0 \tag{1}$$

Second, the local density of optical states ρ can be strongly enhanced in proximity to the plasmonic particle. The scalar field ρ describes the availability of states that a photon emitted from the molecule can populate, forming the physical grounds for the Purcell effect.[28] According to Fermi's golden rule,[29,30] $\gamma_{em} \propto \rho$, and so the plasmon-induced enhancement of ρ causes an increase in γ_{em}. In contrast to free-space, however, not all of the optical states near the plasmonic particle are radiative, some leading to plasmonic quenching, a nonradiative decay process which can be explained by the ohmic losses in the metal particle.[31] We thus split the emission rate γ_{em} into radiative (γ_{rad}) and plasmonically quenched (γ_q) components. The effect of the plasmonic particle on the emission process can then be expressed by the enhancement factors

$$F_{rad} = \frac{\gamma_{rad}}{\gamma^0_{em}}, \quad F_q = \frac{\gamma_q}{\gamma^0_{em}} \tag{2}$$

where γ^0_{em} is the molecule's emission rate without the particle. These two enhancement processes reflect the competing coupling of the molecule's emission to radiative and nonradiative modes of the plasmonic particle. For an idealized spherical nanoparticle, a simple spacial dependence of this coupling can be found, for example, by performing an analytical multipole expansion of the particle's modes.[23,27] For realistic geometries, however, a more complex behavior is expected, requiring an accurate description of the particle's shape.

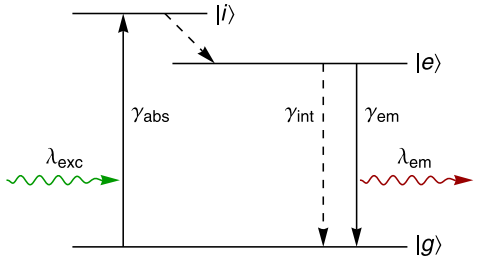

Figure 1. Term diagram of the considered quantum system: ground, intermediate, and excited states $|g\rangle$, $|i\rangle$, and $|e\rangle$, respectively, with radiative (solid lines) and nonradiative transitions (dashed lines).

One should note that while the enhancement factors F describe an influence on the dynamics of a quantum system, they are purely electromagnetic in nature. In no way do they assume a chemical effect on the molecule or a change in the structure of the quantum system, but only manipulation of light. This means that they can be described using classical electrodynamics and, as will be shown below, obtained for arbitrary geometries using classical electromagnetic simulation routines.

Considering that the measurable value in fluorescence or Raman scattering applications is in general the number of photons, or the power, radiated to the far field, we introduce the total rate of radiative decay $\Gamma_{rad} = N_e\gamma_{rad}$, where N_e is the number of molecules in the excited state. The rate equation for N_e can be written as

$$\frac{dN_e}{dt} = N_g\gamma_{abs} - N_e\gamma_{int} - N_e\gamma_{rad} - N_e\gamma_q \tag{3}$$

where N_g is the number of molecules in the ground state. With $N = N_e + N_g$ describing the total number of molecules, the steady-state condition for N_e leads to

$$\Gamma_{rad} = N\frac{\gamma_{abs}\gamma_{rad}}{\gamma_{abs} + \gamma_{int} + \gamma_{rad} + \gamma_q} \tag{4}$$

or, expressed in terms of the enhancement factors,

$$\Gamma_{rad} = N\frac{I^0\tilde{\sigma}F_{exc}\gamma^0_{em}F_{rad}}{I^0\tilde{\sigma}F_{exc} + \gamma^0_{em}(1/\Phi^0_m - 1 + F_{rad} + F_q)} \tag{5}$$

where the molecule's intrinsic free-space quantum yield $\Phi^0_m = \gamma^0_{em}/(\gamma^0_{em} + \gamma_{int})$. The rate of radiative decay without the particle, Γ^0_{rad}, can be computed by setting $F_{exc} = F_{rad} = 1$ and $F_q = 0$. The total enhancement factor G with the particle is then given by $\Gamma_{rad}/\Gamma^0_{rad}$.

Equation 5 can be simplified in certain cases. First, we assume $\Phi^0_m = 1$, so no intrinsic losses. Here, two special

cases can be observed. For weak illumination, a small absorption cross section, or a short-lived excited state, the first term in the denominator in eq 5 can be neglected, and the total rate of radiative decay simplifies to

$$\Gamma_{rad} = NI^0\tilde{\sigma}F_{exc}\Phi_p \quad (6)$$

with the external quantum yield $\Phi_p = F_{rad}/(F_{rad} + F_q)$ of the plasmonic system. In this case, a molecule which is excited immediately decays, either radiatively or nonradiatively, and so $N_g \approx N$. One can see that Γ_{rad} is proportional to the incident intensity I^0, so we call this the linear regime. Without the particle, the total rate of radiative decay in this regime computes to $\Gamma^0_{rad} = NI^0\tilde{\sigma}$ and one can write the total enhancement factor in the linear regime as $G = F_{exc}\Phi_p$.

Conversely, with a high incident intensity, a large absorption cross section or assuming a long-lived excited state, eq 5 simplifies to

$$\Gamma_{rad} = N\gamma^0_{em}F_{rad} \quad (7)$$

Here, the ground state is depleted and Γ_{rad} does not depend on I^0, so we call this the saturation regime. In this case, a high nonradiative decay rate does not affect Γ_{rad} as a molecule which decays nonradiatively will immediately be re-excited and available for radiative decay. Here, without the particle one obtains $\Gamma^0_{rad} = N\gamma^0_{em}$ and the total enhancement factor is simply given by $G = F_{rad}$.

Finally, with a low intrinsic quantum yield, the total rate of radiative decay can be approximated by

$$\Gamma_{rad} = NI^0\tilde{\sigma}\Phi^0_m F_{exc}F_{rad} \quad (8)$$

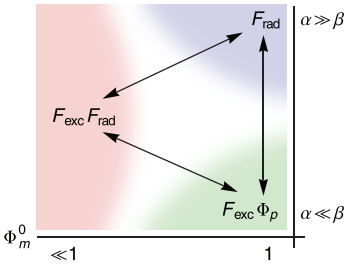

Figure 2. Radiative enhancement factor G in dependence of the factors α, β and Φ^0_m.

The rate of radiative decay without the particle is given by $\Gamma^0_{rad} = NI^0\tilde{\sigma}\Phi^0_m$ for high intrinsic losses, thus the total enhancement factor computes to $G = F_{exc}F_{rad}$.

One can see that the actual fluorescence enhancement G observed near a plasmonic particle depends on the properties of the fluorescent molecule and the plasmonic system as well as the incident intensity. Three regimes can be identified, discriminated by the factors

$$\alpha = \frac{I^0\tilde{\sigma}}{\gamma^0_{em}}, \quad \beta = \frac{F_{rad} + F_q}{F_{exc}} \quad (9)$$

and Φ^0_m. While the factors α and Φ^0_m describe the illuminated quantum system in free space, β depends only on the properties of the plasmonic particle. The described regimes are illustrated in Figure 2.

RESULTS AND DISCUSSION

To estimate the validity domains of the different regimes presented in the previous section, the enhancement factors F_{exc}, F_{rad}, and F_q were calculated numerically for a quantum system (from now on referred to as a "molecule") near a realistic gold nanoparticle, shown in Figure 3a. This particle is largely smooth on its right side and rougher on its left side, allowing a comparison of the effect of roughness on the localized enhancement factors. Simulations were performed using the surface integral equation (SIE) method,[32] and the dielectric constant for gold was taken from experimental data.[33]

First, the resonant behavior of the particle was investigated. Figure 3b shows the particle's normalized scattering cross section C_{sca}, maximum intensity enhancement I_{max}, and mean intensity enhancement I_{mean} for plane-wave illumination at different wavelengths. The illumination scheme is illustrated in Figure 3a. Maximum and mean intensities were calculated on a surface 6 nm from the particle, as suggested by the gray transparent surface shown in Figure 3a. Other polarization settings were also studied but yielded much weaker resonances and can thus be neglected compared to the shown configuration. In this paper, we define the maximum of the scattering cross section as the plasmon resonance, as it is easily

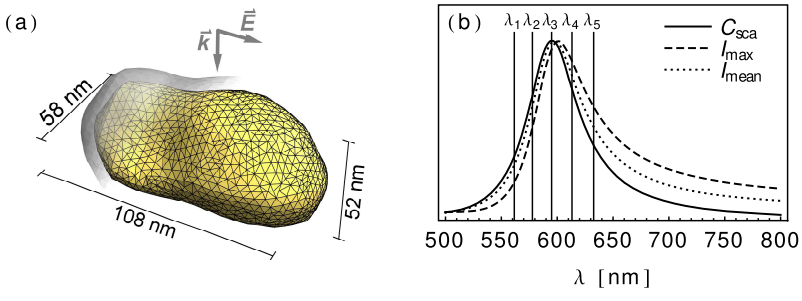

Figure 3. Geometry of plasmonic particle under study (a) and its resonant response (b) for plane wave illumination incident in direction $\vec{k}$ and polarized along $\vec{E}$. Curves in panel b show normalized scattering cross section C_{sca}, maximum intensity enhancement I_{max}, and mean intensity enhancement I_{mean} at points 6 nm from the particle's surface, that is, on the gray transparent surface suggested in panel a.

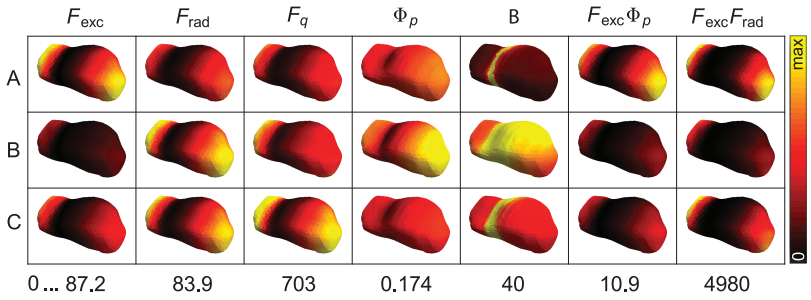

Figure 4. Plasmonic particle-dependent enhancement factors *F* as well as external quantum yield Φ_p and parameter β for a molecule positioned 6 nm above a realistic plasmonic particle, its dipole moment oriented normal to the surface. The right two columns show the total enhancement factor *G* for linear and lossy regimes. A, B, and C denote the tuning configuration (see text). The range plotted in each column is from zero to the value given at the bottom.

accessible in far-field measurements. Because of different damping processes and the onset of retardation effects, the near-field enhancement, which is of primary interest in this study, can in fact be red-shifted with respect to the scattering cross section.[34−37] However, for gold nanorods, this discrepancy has been shown to become important only for rod diameters larger than 100 nm,[34] considerably larger than the 52 or 58 nm dimensions of the particle in this study. Indeed, as can be seen in Figure 3b, the red shift is small compared to the width of the plasmon resonance, and so the error made with this practical assumption can be neglected in our case. For very thick particles or plasmonic systems with narrow resonances, however, a means of more accurately characterizing the near-field enhancement would have to be devised.

As excitation and reemission processes occur at different wavelengths (see Figure 1) the factors F_{rad} and F_q were determined at a wavelength red-shifted from the excitation wavelength by a Stokes-shift of 1000 cm^{-1}. To investigate the effect of tuning the plasmon resonance to the molecular process, three spectral configurations were studied as shown in Table 1.

TABLE 1. Spectral Configurations

tuning	λ_{exc}	λ_{em}	
A	λ_3	λ_5	excitation on resonance
B	λ_1	λ_3	reemission on resonance
C	λ_2	λ_4	centered configuration

Depending on the observed enhancement regime, maximizing the measurable signal means optimizing certain enhancement factors of the plasmonic particle. These values depend on both the wavelength and the position of the molecule relative to the particle. To determine an optimal geometric and spectral configuration, we have plotted in Figure 4 the various enhancement factors for the molecule placed at points 6 nm above the particle's surface. At this distance, the nanoscopic structure of the particle's surface is not reproduced and the field distribution depends on the geometry of the particle as a whole. Closer to the particle,

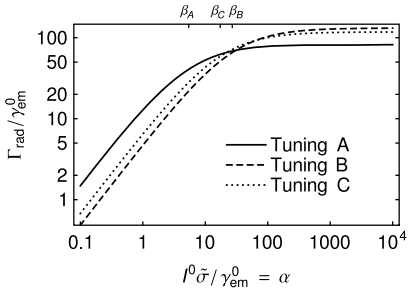

Figure 5. Total rate of radiative decay Γ_{rad} as a function of $I^0\tilde{\sigma}/\gamma^0_{em} = \alpha$. The molecule is located 6 nm from the front-right tip of the particle (see text).

its local topography structure becomes important and must be taken into account in the simulations,[38] as will be discussed below.

In Figure 4, the molecule's dipole moment is assumed to be oriented perpendicular to the surface of the particle. Calculations were also carried out for parallel orientation, but the radiative enhancement factors obtained were orders of magnitude weaker as the image dipole induced in the particle counteracts the molecule's own emission in this orientation. We thus assume normal orientation throughout this paper. For randomly oriented or rotating molecules, the enhancement factors may simply be divided by three.

When calculating the enhancement factors in Figure 4, the appropriate wavelengths were chosen for the spectral tunings A−C, that is, $F_{exc}(\lambda_{exc})$, $F_{rad}(\lambda_{em})$, and $F_{abs}(\lambda_{em})$. From these factors one can then compute Φ_p and β along with the total enhancement factors *G* in the different regimes. In the linear regime, maximizing the measurable signal entails maximizing both the incident intensity enhancement F_{exc} and the quantum yield Φ_p. As Φ_p does not vary greatly between tunings A−C, the enhancement of the incident intensity becomes the primary dependency. Indeed, one can see that tuning A, with the highest value for F_{exc}, yields the highest total enhancement factor $G = F_{exc}\Phi_p$ in the linear regime, even though tuning B has a slightly higher quantum yield. In the saturation regime the total radiative enhancement factor is

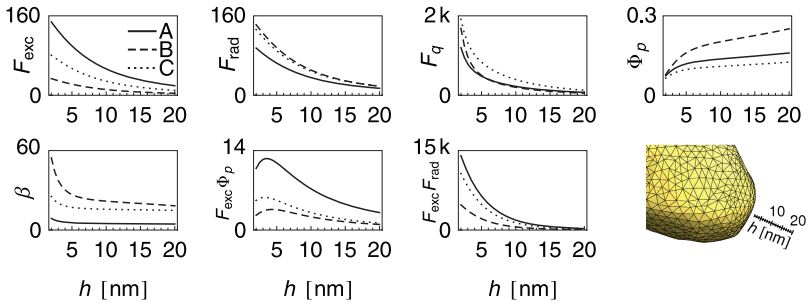

Figure 6. Dependence of the enhancement factors *F* along with the external quantum yield Φ_p and the factor β on the particle−molecule distance *h* (all horizontal axes). The last image shows the positions of the calculated points.

$G = F_{rad}$ and one can see that it is maximized in tuning B, closely followed by tuning C.

Between the two extreme cases of the linear and saturation regimes, the total rate of radiative decay can only be described by the rather complex eq 5 with $\Phi_m^0 = 1$. Intuitively, one might think that Γ_{rad} would be maximal for tuning C as it lies in between the cases A and B. In Figure 5, the total rate of radiative decay is plotted as a function of $I^0\tilde{\sigma}/\gamma_{em}^0 = \alpha$, in units of γ_{em}^0. Here, the molecule is placed $h = 6$ nm from the front-right tip of the gold particle (see Figure 6). The values for the enhancement factors *F* were taken from the simulations, shown in Table 2.

TABLE 2. Values for Enhancement Factors (*F*)

	F_{exc}	F_{rad}	F_q
tuning A	132	82	632
tuning B	30	131	672
tuning C	73	118	1143

One can clearly see the linear and saturation regimes for low and high abscissae, respectively. Also, for $\alpha \approx 30$, the highest value of Γ_{rad} is indeed obtained in tuning C, albeit for a very small region.

It becomes clear that maximizing Γ_{rad} involves taking the molecule's properties into account. If values for $\tilde{\sigma}$ and γ_{em}^0 are known, the correct tuning configuration can be determined using Figure 5. Fluorescent molecules that either have a very short lifetime in their excited state (γ_{em}^0 large) or are difficult to excite ($\tilde{\sigma}$ small) will in general be observed in the linear regime. These are common assumptions made when discussing plasmonic fluorescence enhancement.[25] In this case, it is advantageous to choose a configuration with large enhancement F_{exc} of the incident light and a reasonable quantum yield such as the presented particle in tuning A. If the lifetime is very long (γ_{em}^0 small) or the molecule easy to excite ($\tilde{\sigma}$ large), one will be in the saturation regime and a high enhancement F_{rad} of the radiative decay rate should be aspired, as in tuning B. This configuration is found, for example, when enhancing electric dipole-forbidden transitions.[39] If the used molecule is between the two extremes, one will obtain best results using a configuration like tuning C. If the exact properties of the molecule are not known, tuning C seems to be a good compromise, showing both a large enhancement in saturation and reasonable performance in the linear regime. The modest dependence of the enhancement values on the spectral tuning is in part due to the fact that the width of the plasmon resonance is of the same order as the Stokes-shift. For larger Stokes-shifts, the importance of correct spectral alignment is expected to rise considerably.

Including intrinsic losses in the molecule, that is, $\Phi_m^0 < 1$, the simple cases of the linear and saturation regimes described above are no longer valid. For very lossy systems, however, eq 8 shows a simple dependence of Γ_{rad} on $G = F_{exc}F_{rad}$. Here, the nonradiative losses caused by plasmonic quenching, described by F_q, play no role because their effect is negligible compared to the much higher intrinsic losses. The factor *G* for lossy systems is shown in the rightmost column in Figure 4 for spectral tunings A, B, and C. Reciprocity demands that the two factors F_{exc} and F_{rad} be the same for a plasmon resonance tuned to their respective wavelength (F_{exc} at tuning A is equal to F_{rad} at tuning B).[38] Owing to the asymmetry of the plasmon resonance curve shown in Figure 3, especially in the near-field, however, the respective other factors are in fact different when shifting the plasmon resonance. Indeed, one can see that F_{exc} is much lower for tuning B than F_{rad} for tuning A. This leads to an optimal spectral configuration of tuning A for the case of large intrinsic losses.

Next, we are interested in the dependence of Γ_{rad} for different particle−molecule separations. In Figure 4 and Figure 5, a fixed distance of 6 nm was chosen. The enhancement factors *F* along with Φ_p and β are now calculated for distances between 2 and 20 nm from the particle's surface, shown in Figure 6. The front-right tip of the plasmonic particle was again chosen for the position of the molecule. One can see that all the enhancement factors *F* increase monotonously as one nears the particle. However, as both F_{rad} and F_q compete in the quantum yield Φ_p, the rapid increase in F_q causes a steep decrease in Φ_p for $h < 5$ nm. Consequently, the initially rising linear enhancement factor $F_{exc}\Phi_p$ culminates in a maximum at around $h = 3$ nm from the surface before decreasing again as one

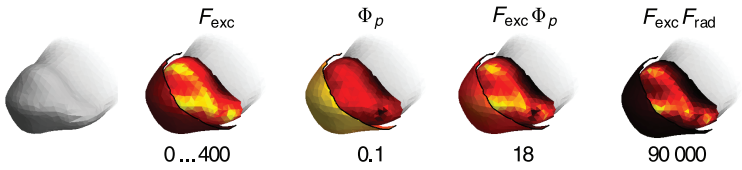

Figure 7. Geometry and enhancement parameters around the left, rough end of the plasmonic particle. Factors are shown in tuning A for distances h = 1 nm (inner surface) and h = 6 nm (outer, clipped surface) above the particle's surface. Scaled as in Figure 4.

further nears the particle. In the linear regime, the optimal configuration is thus not on the surface itself, but at a small distance from the particle, before fluorescence quenching becomes dominant. For decreasing quantum yields, the optimal distance h moves closer to the particle.[40] Finally, in the limit of $\Phi_m^0 \rightarrow 0$, that is, the lossy regime, as well as in the saturation regime, the closer one is to the particle, the more light is radiated to the far field as quenching plays no role.

The optimal distance from the scatterer accordingly depends on the type of molecule under study. For quickly decaying fluorophores, we can infer that it is best to place the molecule at a distance from the particle's surface. This localization can be performed, for example, *via* surface functionalization. For slowly decaying molecules or such with large intrinsic losses, on the other hand, the total radiated power is maximized if the particle is as close to the surface as possible. It is thus best to deposit such molecules directly on or very close to the surface of the enhancing particle.

The distance-dependence of the enhancement factor has a direct effect on the optimal geometric configuration of the particle–molecule system. In a previous study we have shown that for distances over h = 5 nm from the surface of a plasmonic nanoparticle, the field enhancement no longer depends on the nanoscopic topography of the particle.[38] Likewise, the enhancement distributions in Figure 4, at h = 6 nm, display no effects of the realistic surface of the modeled nanoparticle, showing only the characteristic response of a dipole antenna. The distance dependence shown in Figure 6, recorded over the smooth, right end of the particle, also shows similar behavior as reported for idealized, perfectly smooth structures.[25,26] We conclude that for large enough distances from the particle or sufficiently smooth surfaces, calculations with idealized geometries will yield accurate results.

Turning to the left, rougher end of the studied particle, however, we can see that the particle's realistic shape can in fact have a large impact on the enhancement processes. Figure 7 shows the geometry and enhancement parameters calculated in tuning A for distances h = 1 nm (inner surface) and h = 6 nm (outer, clipped surface) above the particle's surface. Two remarkable features can be seen in this representation. First, for h = 1 nm, the surface roughness induces very localized and intense regions of field enhancement, yielding values of F_{exc} much higher than for a smooth surface. Interestingly, the plasmonic quantum yield Φ_p does not reproduce the surface topography, though it does decrease for smaller h as expected. Evidently, the coupling to nonradiative modes experiences a similar enhancement by the roughness as the coupling to radiative modes. Second, in those regions of strong incident field enhancement, the total linear-regime enhancement $G = F_{exc}\Phi_p$ takes on unexpectedly high values. At a distance of h = 1 nm, a molecule operating in the linear regime would be expected to be nearly totally quenched.[25] The surface roughness, however, can cause fluorescence enhancement stronger even than for optimal placement over a smooth particle. In the saturation and lossy regimes, as well, the roughness causes localized areas of extremely large enhancement. It becomes clear that an accurate geometrical description of the nanoparticle is absolutely imperative unless the plasmonic particles under study are completely smooth or the molecule is prevented from reaching the particle's surface.

In an experimental system, it can be difficult to completely immobilize a molecule, thus its position around a plasmonic particle may vary with time. The impact of this spacial uncertainty can be directly extracted from Figure 4 and Figure 7: At distances close to the particle, the molecule's localization should be as rigid as possible, as a shift of even few nanometers can move the molecule out of a hot spot, immediately reducing the enhancement. Farther away, the molecule's immobilization is no longer critical, as the enhancement factors do not change considerably over tens of nanometers.

Until now, the radiative enhancement of fluorescent molecules with different properties has been discussed. To extend this study to the enhancement of Raman scattering, one might think it would suffice to choose an appropriately small excited lifetime, that is, a very high γ_{em}^0, as the excited state is virtual. However, with an interpretation of Raman scattering as a combination of absorption and reemission, the two can no longer be completely separated. Instead, conventional (nonresonance) Raman scattering (considering a particular vibrational mode) can be interpreted as two dipoles at the excitation, respectively, the scattering wavelengths, coupled to have the same dipole moment $\vec{p}$.[41] Driven in the excitation field $\vec{E}_{exc}$, one can write

$$\vec{p} = \alpha \cdot \vec{E}_{exc} \qquad (10)$$

where α is a polarizability tensor and, barring chemical effects as the molecule nears the metallic particle, independent of the position. The Raman-scattered light is then the light radiated by the corresponding dipole at the scattered wavelength in the plasmonic system. The excitation and emission properties of a dipole lead to the well-known Raman enhancement factor[42]

$$G = F_{exc}(\lambda_{exc})\, F_{rad}(\lambda_{em}) \qquad (11)$$

This factor describes the power of the Raman-scattered light radiated to the far field with the molecule in the plasmonic system compared to one in free-space, considering identical illumination. Immediately, one can see that G is the same as in the lossy regime: Raman scattering is enhanced by the same factor as a fluorescent molecule with a very poor intrinsic quantum yield. This is not unexpected as Raman scattering is often compared to fluorescence by a very poor emitter.[22,23,43]

From Figure 6 we can deduce that the highest nonresonance Raman enhancement is obtained if excitation is performed at the resonance wavelength of the plasmonic particle. This prediction is supported by numerous experimental studies.[44,45] Haynes *et al.* deduce that the enhancement factor is the greatest for λ_{max} inside a window of ~120 nm containing both the excitation and scattering wavelengths. However, this simply corresponds to the width of the plasmon resonance and high enhancement factors are, in fact, measured in particular if the plasmon resonance coincides with the excitation wavelength (*cf.* Figure 5 in the study,[44] $\lambda_{max} \approx \lambda_{ex}$), for which we also predict best performance. Although these measurements contain considerable uncertainties like particle size, shape, and molecule location, the obtained optimal configuration is in agreement with our result. Conversely, if maximizing the scattered intensity is not essential, tuning the plasmon resonance of the particle to the scattered wavelength allows selective enhancement of a particular mode in a broadband Raman spectrum.[42]

In resonance Raman scattering, quenching is not completely absent as the coherent oscillations of the molecular dipole excited by the incident field can couple to modes of a nearby plasmonic particle.[27] Typically, the dephasing rate κ of the near-resonantly excited molecular dipole is much larger than the decay rate of the near-resonant transition's excited state.[46] In this case, the enhancement of the Raman process behaves just like that of a fluorescent system with an intrinsic quantum yield of $\Phi_m^0 = 2\gamma_{em}^0/\kappa$.[22] The enhancement of Raman scattering is thus equivalent to that of a lossy fluorophore, with conventional Raman scattering corresponding to the limit $\Phi_m^0 \to 0$.

With the given framework, the enhancement factors for various types of molecules can be determined for realistic geometries. This will aid in the design and characterization of structures optimized to yield the highest fluorescence or Raman signal. Using numerical simulations or near-field microscopy[47−49] to characterize the structures alone, the theory presented above can also be used to gain additional information about a molecule: Given the factor β around a plasmonic particle, the regime in which a nearby molecule is enhanced is a measure for α or Φ_m^0 and can be used to estimate the molecule's transition rates or intrinsic quantum yield.

The presented theoretical description can also prove useful for interpreting experimental results obtained in apertureless near-field microscopy.[6,50,51] In this approach, the plasmonic particle is replaced by a metallic tip which can be moved around a sample with high precision. Inserting the well-defined geometric configuration into the presented framework along with the bare tip's response obtained from numerical simulations,[52−54] the near-field optical image obtained from this method can be further analyzed to yield the sample's quantum yield or transition rates. In a near-field study on an organic semiconductor (diindenoperylene, DIP) thin film,[21] for example, both the obtained enhancement factor and its tip−sample distance dependence could be used to predict a very low quantum yield $\Phi_m^0 \approx 10^{-3}$ of the DIP molecules. Indeed, previous studies have reported quantum yields in the percent range for crystalline films of perylene chromophores like DIP due to an exciton dispersion with a minimum at the surface of the Brillouin zone.[55]

CONCLUSION

In this paper, an expression for the total rate of radiative decay of a fluorophore near a plasmonic particle was derived, taking into account the Stokes-shift, the quantum yield, and the rates of the observed transition. It could be shown that, depending on the properties of the molecule under study, the enhancement factor could be described by one of many different expressions. Numerical investigation of the photonic environment of a realistic gold nanoparticle showed that different molecules will experience enhancement factors varying by many orders of magnitude. In addition, the optimal spacial and spectral configuration of the molecule/particle system is strongly dependent on the molecular transition's properties. Taking the particle's surface roughness into account, it could be shown that very localized areas of field enhancement can lead to fluorescence enhancement under conditions otherwise predicted to completely quench the emitter.

These results shed new light on the enhancement of radiative processes using plasmonic particles. It was shown that a single optimal configuration cannot be found for all types of molecules, but that both the particle and the position of the molecule must be engineered according to the molecule's properties. A sound understanding of the different enhancement

strengths will not only lead to structures with optimized performance, but can also yield new techniques for measuring the intrinsic properties of fluorescent or Raman-active molecules.

METHODS

The three-dimensional simulations in this study were performed using the surface integral equation (SIE) method.[32] In this approach, homogeneous bodies are discretized on their surface only, minimizing the complexity of the calculations. The unstructured mesh is capable of describing highly irregular structures, while continuous basis functions ensure the physicality of the obtained fields arbitrarily close to the particle's surface. The dielectric function for gold was taken from experimental data[33] and interpolated to the required wavelengths. The particle's geometry was derived from a scanning electron microscope (SEM) image of an actual gold nanoantenna.[38]

The enhancement factors F can be directly obtained from the electromagnetic simulation results. The excitation enhancement F_{exc} is simply the intensity near the particle upon illumination with a unit amplitude plane wave. The emission enhancement factors F_{rad} and F_q are determined by placing a dipole emitter near the particle, at positions for which the factors are to be computed. Next, the powers radiated to the far field and absorbed by the particle are calculated,

$$P_{rad} = \int_A \hat{n}(\vec{r}) \cdot \vec{S}(\vec{r})\, dS \tag{12}$$

and

$$P_{abs} = -\int_{\partial\Omega} \hat{n}(\vec{r}) \cdot \vec{S}(\vec{r})\, dS \tag{13}$$

respectively. Here, A is a closed surface containing both the emitter and the particle, $\partial\Omega$ is the particle's surface, $\hat{n}(\vec{r})$ is the outward facing normal vector and $\vec{S}(\vec{r}) = \mathcal{R}\{\vec{E}(\vec{r}) \times \vec{H}^*(\vec{r})\}/2$ is the Poynting vector.[56] The enhancement factors are then obtained by comparison to the power P_{dip} emitted by a dipole in free space,

$$F_{rad} = \frac{P_{rad}}{P_{dip}}, \quad F_q = \frac{P_{abs}}{P_{dip}} \tag{14}$$

with $P_{dip} = p^2\omega^4\mu/(12\pi c)$. Here, p is the emitter's dipole moment, ω is its angular frequency, μ is the surrounding space's magnetic permeability, and c is the speed of light therein.

The enhancement factor for resonance Raman scattering, G_{RRS}, can be derived from the study by Weitz *et al.*,[22] eqs (28) and (32). Taking the limits of near-resonant excitation and fast dephasing ($\kappa \gg \gamma^0_{em}$), one can write

$$G_{RRS} = \frac{1}{\left(1 + \frac{\gamma^0_{em}}{\kappa}(F_{rad} + F_q - 1)\right)^2} F_{exc} F_{rad} \tag{15}$$

Substituting $\eta = 2\gamma^0_{em}/\kappa$ and assuming $\eta(F_{rad} + F_q - 1) \ll 1$, that is, dephasing is much faster than even the plasmonically enhanced decay, eq 15 becomes

$$G_{RRS} = \frac{\eta^{-1}}{\eta^{-1} - 1 + F_{rad} + F_q} F_{exc} F_{rad} \tag{16}$$

With $\Phi^0_m = \eta$, this is the same enhancement factor as obtained for weak emitters.

Conflict of Interest: The authors declare no competing financial interest.

Acknowledgment. This work was supported by the Swiss National Science Foundation (Grant 20021-116758), the German Academic Exchange Service and the Deutsche Forschungsgemeinschaft (Project 14043013).

REFERENCES AND NOTES

1. Jeanmaire, D. L.; Van Duyne, R. P. Surface Raman Spectroelectrochemistry: Part I. Heterocyclic, Aromatic, and Aliphatic Amines Adsorbed on the Anodized Silver Electrode. *J. Electroanal. Chem. Interface* **1977**, *84*, 1–20.
2. Moskovits, M. Surface-Enhanced Spectroscopy. *Rev. Mod. Phys.* **1985**, *57*, 783–826.
3. Kneipp, K.; Wang, Y.; Kneipp, H.; Perelman, L. T.; Itzkan, I.; Dasari, R. R.; Feld, M. S. Single Molecule Detection Using Surface-Enhanced Raman Scattering (SERS). *Phys. Rev. Lett.* **1997**, *78*, 1667–1670.
4. Nie, S.; Emory, S. R. Probing Single Molecules and Single Nanoparticles by Surface-Enhanced Raman Scattering. *Science* **1997**, *275*, 1102–1106.
5. Xie, X. S.; Trautman, J. K. Optical Studies of Single Molecules at Room Temperature. *Annu. Rev. Phys. Chem.* **1998**, *49*, 441–480.
6. Stöckle, R. M.; Suh, Y. D.; Deckert, V.; Zenobi, R. Nanoscale Chemical Analysis by Tip-Enhanced Raman Spectroscopy. *Chem. Phys. Lett.* **2000**, *318*, 131–136.
7. Matterson, B. J.; Lupton, J. M.; Safonov, A. F.; Salt, M. G.; Barnes, W. L.; Samuel, I. D. W. Increased Efficiency and Controlled Light Output from a Microstructured Light-Emitting Diode. *Adv. Mater.* **2001**, *13*, 123–127.
8. Mulvaney, S. P.; Musick, M. D.; Keating, C. D.; Natan, M. J. Glass-Coated, Analyte-Tagged Nanoparticles: A New Tagging System Based on Detection with Surface-Enhanced Raman Scattering. *Langmuir* **2003**, *19*, 4784–4790.
9. Talley, C. E.; Jackson, J. B.; Oubre, C.; Grady, N. K.; Hollars, C. W.; Lane, S. M.; Huser, T. R.; Nordlander, P.; Halas, N. J. Surface-Enhanced Raman Scattering from Individual Au Nanoparticles and Nanoparticle Dimer Substrates. *Nano Lett.* **2005**, *5*, 1569–1574.
10. Demming, A. L.; Festy, F.; Richards, D. Plasmon Resonances on Metal Tips: Understanding Tip-Enhanced Raman Scattering. *J. Chem. Phys.* **2005**, *122*, 184716.
11. Lakowicz, J. R. Radiative Decay Engineering 5: Metal-Enhanced Fluorescence and Plasmon Emission. *Anal. Biochem.* **2005**, *337*, 171–194.
12. Kühn, S.; Håkanson, U.; Rogobete, L.; Sandoghdar, V. Enhancement of Single-Molecule Fluorescence Using a Gold Nanoparticle as an Optical Nanoantenna. *Phys. Rev. Lett.* **2006**, *97*, 017402.
13. Schatz, G.; Young, M.; Van Duyne, R. Electromagnetic Mechanism of SERS. In *Surface-Enhanced Raman Scattering*; Kneipp, K., Moskovits, M., Kneipp, H., Eds.; Springer: Berlin/Heidelberg, 2006; Vol. 103, pp 19–45.
14. Lakowicz, J. R.; Ray, K.; Chowdhury, M.; Szmacinski, H.; Fu, Y.; Zhang, J.; Nowaczyk, K. Plasmon-Controlled Fluorescence: A New Paradigm in Fluorescence Spectroscopy. *Analyst* **2008**, *133*, 1308–1346.
15. Zoriniants, G.; Barnes, W. L. Fluorescence Enhancement through Modified Dye Molecule Absorption Associated with the Localized Surface Plasmon Resonances of Metallic Dimers. *New J. Phys.* **2008**, *10*, 105002.
16. Li, J. F.; Huang, Y. F.; Ding, Y.; Yang, Z. L.; Li, S. B.; Zhou, X. S.; Fan, F. R.; Zhang, W.; Zhou, Z. Y.; Wu, D. Y. Shell-Isolated Nanoparticle-Enhanced Raman Spectroscopy. *Nature* **2010**, *464*, 392–395.
17. Mackowski, S.; Wormke, S.; Maier, A. J.; Brotosudarmo, T. H. P.; Harutyunyan, H.; Hartschuh, A.; Govorov, A. O.; Scheer, H.; Brauchle, C. Metal-Enhanced Fluorescence of Chlorophylls in Single Light-Harvesting Complexes. *Nano Lett.* **2008**, *8*, 558–564.
18. Govorov, A. O.; Carmeli, I. Hybrid Structures Composed of Photosynthetic System and Metal Nanoparticles: Plasmon Enhancement Effect. *Nano Lett.* **2007**, *7*, 620–625.

19. Beyer, S. R.; Ullrich, S.; Kudera, S.; Gardiner, A. T.; Cogdell, R. J.; Koehler, J. Hybrid Nanostructures for Enhanced Light-Harvesting: Plasmon Induced Increase in Fluorescence from Individual Photosynthetic Pigment−Protein Complexes. *Nano Lett.* **2011**, *11*, 4897–4901.
20. Anker, J. N.; Hall, W. P.; Lyandres, O.; Shah, N. C.; Zhao, J.; Van Duyne, R. P. Biosensing with Plasmonic Nanosensors. *Nat. Mater.* **2008**, *7*, 442–453.
21. Zhang, D.; Heinemeyer, U.; Stanciu, C.; Sackrow, M.; Braun, K.; Hennemann, L. E.; Wang, X.; Scholz, R.; Schreiber, F.; Meixner, A. J. Nanoscale Spectroscopic Imaging of Organic Semiconductor Films by Plasmon−Polariton Coupling. *Phys. Rev. Lett.* **2010**, *104*, 056601.
22. Weitz, D. A.; Garoff, S.; Gersten, J. I.; Nitzan, A. The Enhancement of Raman Scattering, Eesonance Raman Scattering, and Fluorescence from Molecules Adsorbed on a Rough Silver Surface. *J. Chem. Phys.* **1983**, *78*, 5324–5338.
23. Pettinger, B. Light Scattering by Adsorbates at Ag Particles: Quantum-Mechanical Approach for Energy Transfer Induced Interfacial Optical Processes Involving Surface Plasmons, Multipoles, and Electron-Hole Pairs. *J. Chem. Phys.* **1986**, *85*, 7442–7451.
24. Des Francs, G. C.; Girard, C.; Laroche, T.; Lévèque, G.; Martin, O. J. F. Theory of Molecular Excitation and Relaxation near a Plasmonic Device. *J. Chem. Phys.* **2007**, *127*, 034701.
25. Anger, P.; Bharadwaj, P.; Novotny, L. Enhancement and Quenching of Single-Molecule Fluorescence. *Phys. Rev. Lett.* **2006**, *96*, 113002.
26. Sun, G.; Khurgin, J. B.; Soref, R. A. Practical Enhancement of Photoluminescence by Metal Nanoparticles. *Appl. Phys. Lett.* **2009**, *94*, 101103.
27. Sun, G.; Khurgin, J. B. Origin of Giant Difference between Fluorescence, Resonance, and Nonresonance Raman Scattering Enhancement by Surface Plasmons. *Phys. Rev. A* **2012**, *85*, 063410.
28. Purcell, E. M. Spontaneous Emission Probabilities at Radio Frequencies. *Phys. Rev.* **1946**, *69*, 37–38.
29. Agarwal, G. S. Vacuum-Field Rabi Oscillations of Atoms in a Cavity. *J. Opt. Soc. Am. B* **1985**, *2*, 480–485.
30. Cohen-Tannoudji, C.; Dupont-Roc, J.; Grynberg, G. *Atom-Photon Interactions*; Wiley: Weinheim, Germany, 2004.
31. Bian, R. X.; Dunn, R. C.; Xie, X. S.; Leung, P. T. Single Molecule Emission Characteristics in Near-Field Microscopy. *Phys. Rev. Lett.* **1995**, *75*, 4772–4775.
32. Kern, A. M.; Martin, O. J. F. Surface Integral Formulation for 3D Simulations of Plasmonic and High Permittivity Nanostructures. *J. Opt. Soc. Am. A* **2009**, *26*, 732–740.
33. Johnson, P. B.; Christy, R. W. Optical Constants of the Noble Metals. *Phys. Rev. B* **1972**, *6*, 4370–4379.
34. Bryant, G. W.; Garcia de Abajo, F. J.; Aizpurua, J. Mapping the Plasmon Resonances of Metallic Nanoantennas. *Nano Lett.* **2008**, *8*, 631–636.
35. Pfeiffer, M.; Lindfors, K.; Wolpert, C.; Atkinson, P.; Benyoucef, M.; Rastelli, A.; Schmidt, O. G.; Giessen, H.; Lippitz, M. Enhancing the Optical Excitation Efficiency of a Single Self-Assembled Quantum Dot with a Plasmonic Nanoantenna. *Nano Lett.* **2010**, *10*, 4555–4558.
36. Zuloaga, J.; Nordlander, P. On the Energy Shift between Near-Field and Far-Field Peak Intensities in Localized Plasmon Systems. *Nano Lett.* **2011**, *11*, 1280–1283.
37. Chen, J.; Albella, P.; Pirzadeh, Z.; Alonso-González, P.; Huth, F.; Bonetti, S.; Bonanni, V.; Åkerman, J.; Nogués, J.; Vavassori, P. Plasmonic Nickel Nanoantennas. *Small* **2011**, *7*, 2341–2347.
38. Kern, A. M.; Martin, O. J. F. Excitation and Reemission of Molecules near Realistic Plasmonic Nanostructures. *Nano Lett.* **2011**, *11*, 482–487.
39. Kern, A. M.; Martin, O. J. F. Strong Enhancement of Forbidden Atomic Transitions using Plasmonic Nanostructures. *Phys. Rev. A* **2012**, *85*, 022501.
40. Sun, G.; Khurgin, J. B.; Yang, C. C. Impact of High-Order Surface Plasmon Modes of Metal Nanoparticles on Enhancement of Optical Emission. *Appl. Phys. Lett.* **2009**, *95*, 171103.
41. Kerker, M. Estimation of Surface-Enhanced Raman Scattering from Surface-Averaged Electromagnetic Intensities. *J. Colloid Interface Sci.* **1987**, *118*, 417–421.
42. Zhang, W.; Fischer, H.; Schmid, T.; Zenobi, R.; Martin, O. J. F. Mode-Selective Surface-Enhanced Raman Spectroscopy Using Nanofabricated Plasmonic Dipole Antennas. *J. Phys. Chem. C* **2009**, *113*, 14672–14675.
43. Xu, H.; Wang, X.-H.; Persson, M. P.; Xu, H. Q.; Käll, M.; Johansson, P. Unified Treatment of Fluorescence and Raman Scattering Processes near Metal Surfaces. *Phys. Rev. Lett.* **2004**, *93*, 243002.
44. Haynes, C. L.; Van Duyne, R. P. Plasmon-Sampled Surface-Enhanced Raman Excitation Spectroscopy. *J. Phys. Chem. B* **2003**, *107*, 7426–7433.
45. Jackson, J. B.; Halas, N. J. Surface-Enhanced Raman Scattering on Tunable Plasmonic Nanoparticle Substrates. *Proc. Natl. Acad. Sci. U.S.A.* **2004**, *101*, 17930–17935.
46. Lawless, M. K.; Mathies, R. A. Excited-State Structure and Electronic Dephasing Time of Nile Blue from Absolute Resonance Raman Intensities. *J. Chem. Phys.* **1992**, *96*, 8037–8045.
47. Pohl, D. W.; Denk, W.; Lanz, M. Optical Stethoscopy: Image Recording with Resolution $\lambda/20$. *Appl. Phys. Lett.* **1984**, *44*, 651–653.
48. Betzig, E.; Isaacson, M.; Lewis, A. Collection Mode Near-Field Scanning Optical Microscopy. *Appl. Phys. Lett.* **1987**, *51*, 2088–2090.
49. Chicanne, C.; David, T.; Quidant, R.; Weeber, J. C.; Lacroute, Y.; Bourillot, E.; Dereux, A.; Colas des Francs, G.; Girard, C. Imaging the Local Density of States of Optical Corrals. *Phys. Rev. Lett.* **2002**, *88*, 097402.
50. Sackrow, M.; Stanciu, C.; Lieb, M. A.; Meixner, A. J. Imaging Nanometre-Sized Hot Spots on Smooth Au Films with High-Resolution Tip-Enhanced Luminescence and Raman Near-Field Optical Microscopy. *ChemPhysChem* **2008**, *9*, 316–320.
51. Sevinc, P. C.; Wang, X.; Wang, Y.; Zhang, D.; Meixner, A. J.; Lu, H. P. Simultaneous Spectroscopic and Topographic Near-Field Imaging of TiO_2 Single Surface States and Interfacial Electronic Coupling. *Nano Lett.* **2011**, *11*, 1490–1494.
52. Zhang, W.; Cui, X.; Martin, O. J. F. Local Field Enhancement of an Infinite Conical Metal Tip Illuminated by a Focused Beam. *J. Raman Spectrosc.* **2009**, *40*, 1338–1342.
53. Chen, W.; Zhan, Q. Numerical Study of an Apertureless Near Field Scanning Optical Microscope Probe Under Radial Polarization Illumination. *Opt. Express* **2007**, *15*, 4106–4111.
54. Bouhelier, A.; Renger, J.; Beversluis, M. R.; Novotny, L. Plasmon-Coupled Tip-Enhanced Near-Field Optical Microscopy. *J. Microsc.* **2003**, *210*, 220–224.
55. Nollau, A.; Hoffmann, M.; Floreck, K.; Fritz, T.; Leo, K. A Simple Measurement of the Absolute Internal Quantum Efficiency of Thin Organic Films. *J. Appl. Phys.* **2000**, *87*, 7802–7804.
56. Kern, A. M.; Martin, O. J. F. Pitfalls in the Determination of Optical Cross Sections from Surface Integral Equation Simulations. *IEEE Trans. Antennas Propag.* **2010**, *58*, 2158–2161.